

Radio Science



RESEARCH ARTICLE

10.1029/2024RS008156

Key Points:

- Effectiveness of integrating metasurface (MTS) layer to enhance antenna performance is investigated and validated by optical ray tracing analysis
- Introduction of the MTS layer resulted in a more highly directional beamwidth and making its beam more focused
- MTS layer decreases the total internal reflection of incident rays causing to reduce signal loss and improving overall system performance

Correspondence to:

M. Alibakhshikenari and T. A. Elwi, mohammad.alibakhshikenari@universityofgalway.ie; taelwi82@gmail.com

Citation:

Shabeeb Kamil, A., Mousa Ali, E., Alibakhshikenari, M., Misran, N., Tariqul Islam, M., Virdee, B., et al. (2025). Metasurface effect on the performance of planar antennas for wireless communications. *Radio Science*, 60, e2024RS008156. https://doi.org/10.1029/ 2024RS008156

Received 24 OCT 2024 Accepted 12 OCT 2025

Author Contributions:

Conceptualization: Amenah Shabeeb Kamil, Esraa Mousa Ali, Mohammad Alibakhshikenari, Norbahiah Misran, Bal Virdee, Taha A. Elwi

Data curation: Amenah Shabeeb Kamil, Esraa Mousa Ali, Norbahiah Misran, Mohammad Tariqul Islam, Taha A. Elwi Formal analysis:

Mohammad Alibakhshikenari, Norbahiah Misran, Mohammad Tariqul Islam, Bal Virdee, Dion Mariyanayagam Funding acquisition:

Mohammad Alibakhshikenari Investigation: Esraa Mousa Ali, Mohammad Alibakhshikenari, Norbahiah Misran, Bal Virdee, Dion Mariyanayagam, Nisar Ahmad Abbasi

© 2025. The Author(s).

This is an open access article under the terms of the Creative Commons

Attribution License, which permits use, distribution and reproduction in any medium, provided the original work is properly cited.

Metasurface Effect on the Performance of Planar Antennas for Wireless Communications

Amenah Shabeeb Kamil¹, Esraa Mousa Ali², Mohammad Alibakhshikenari^{3,4} , Norbahiah Misran¹, Mohammad Tariqul Islam¹, Bal Virdee⁵ , Dion Mariyanayagam⁵ , Nisar Ahmad Abbasi⁶, Nasr Rashid^{7,8} , and Taha A. Elwi⁹

¹Department of Electrical, Electronic and Systems Engineering, Faculty of Engineering and Built Environment, Universiti Kebangsaan Malaysia (UKM), Bangi, Malaysia, ²Communications and Computer Engineering Department, Al-Ahliyya Amman University, Amman, Jordan, ³LERO, the Research Ireland Centre for Software, College of Science and Engineering, School of Computer Science, University of Galway, Galway, Ireland, ⁴Department of Electrical and Electronics Engineering, Dogus University, Istanbul, Türkey, ⁵Center for Communications Technology, London Metropolitan University, London, UK, ⁶Department of Electrical Engineering, School of Systems Engineering, Bahrain Polytechnic, Isa Town, Bahrain, ⁷Electrical Engineering Department, College of Engineering, Jouf University, Sakaka, Aljouf, Saudi Arabia, ⁸Department of Electrical Engineering, Faculty of Engineering, Al-Azhar University, Nasr City, Egypt, ⁹Department of Automation and Artificial Intelligence Engineering, College of Information Engineering, Al-Nahrain University, Baghdad, Iraq

Abstract This paper demonstrates the performance enhancement of a conventional planar antenna by incorporating metasurface (MTS) layer using a proposed unit-cell array. The impact of MTS unit-cell density on bit-error-rate (BER) and channel capacity (CC) in a point-to-point microwave link is investigated. The MTS layer is constructed from an array of identical unit-cells, including circular, square, and Jerusalem cross microstrip-line elements. The proposed H-shaped checkerboard antenna design is integrated with the MTS and evaluated for various unit-cell densities. Analytical scrutiny reveals significant enhancements in BER and CC with higher MTS unit-cell density, along with an increase in antenna gain through optimal MTS placement. This improvement is attributed to the MTS's ability to concentrate radiated energy within a narrower spatial region, optimizing signal transmission. Experimental validation shows a strong correlation between analytical predictions and measured results, confirming the effectiveness of our methodology. This study not only highlights the impact of MTS configurations on wireless channel performance but also provides valuable insights into the design and optimization of future wireless communication systems.

1. Introduction

The escalating need for high capacity and speed in wireless communications has spurred rapid advancements in telecommunication systems (Elsharief et al., 2022; Etman et al., 2025; Tantawy et al., 2024). Current and forthcoming 5G systems demand heightened throughput and performance enhancements (Glover & Grant, 2010; Iskandarani, 2024; Qasem, 2024). To meet these demands while minimizing interference effects, novel antenna designs are imperative (Alibakhshikenari, Babaeian, et al., 2020; Alibakhshikenari, Virdee, et al., 2020; Alibakhshikenari et al., 2022). Consequently, a plethora of research studies have proposed new antenna array topologies (Henthorn et al., 2017a, 2017b). Modern wireless communication systems increasingly rely on antenna arrays, multi-beam antennas, and beamforming technology (Babakhani et al., 2008). Various antenna technologies are leveraged in 5G devices to optimize efficiency, gain, and capacity (Babakhani et al., 2008; Elsharief et al., 2022; Etman et al., 2025; Glover & Grant, 2010; Qasem, 2024; Tantawy et al., 2024).

In addition to 5G, metasurface-based antennas have gained significant attention in other domains such as the Internet of Things (IoT), satellite communications, and biomedical telemetry systems. Their ability to enable compact, reconfigurable, and high-gain designs makes them suitable for space-constrained and performance-critical applications across a wide range of frequency bands (Chen et al., 2021; Kiani et al., 2022; Yang et al., 2020).

For instance, (Park et al., 2016) proposes printed circuits with metamaterial microstrip antennas featuring beam steering technology for 5G devices. Similarly, (Manteghi, 2016) introduces an electrically large microstrip patch

SHABEEB KAMIL ET AL. 1 of 15



Methodology: Amenah Shabeeb Kamil, Mohammad Alibakhshikenari, Bal Virdee, Dion Mariyanayagam, Nasr Rashid Project administration: Mohammad Alibakhshikenari

Resources: Amenah Shabeeb Kamil, Esraa Mousa Ali.

Mohammad Alibakhshikenari, Norbahiah Misran, Nasr Rashid,

Software: Amenah Shabeeb Kamil, Esraa Mousa Ali, Mohammad Alibakhshikenari,

Norbahiah Misran

Supervision:

Taha A. Elwi

Mohammad Alibakhshikenari **Validation:** Amenah Shabeeb Kamil, Esraa Mousa Ali, Mohammad Alibakhshikenari, Norbahiah Misran, Mohammad Tariqul Islam, Bal Virdee, Dion Mariyanayagam, Nisar Ahmad Abbasi, Nasr Rashid.

Taha A. Elwi Visualization:

Mohammad Alibakhshikenari, Mohammad Tarigul Islam, Bal Virdee.

Nisar Ahmad Abbasi, Nasr Rashid, Taha A. Elwi

Writing - original draft:

Amenah Shabeeb Kamil, Esraa Mousa Ali, Norbahiah Misran

Writing - review & editing:

Mohammad Alibakhshikenari, Mohammad Tariqul Islam, Bal Virdee, Dion Mariyanayagam, Nisar Ahmad Abbasi, Nasr Rashid, Taha A. Elwi antenna with a periodic three-dimensional split-ring resonator structure to maintain high beam directivity and minimize side lobes.

In the field of massive multiple-input multiple-output (MIMO) systems operating at sub-6 GHz bands, (Henthorn et al., 2017a, 2017b) proposes a metasurface (MTS) lens-antenna with large dimensions. This lens-antenna is designed to split the antenna beam for 5G networks at 3.5 GHz.

Moreover, (Abdelrahman et al., 2017) presents a hybrid MTS layer aimed at frequency reconfiguration by etching a C-shaped slot defect from a partial ground plane on the opposite side of a square patch. In biomedical applications, (Balanis, 2016) describes a fractal antenna design in the 1.8 GHz frequency band to control antenna radiation patterns. For beam focusing enhancement purposes, (Babakhani et al., 2008) proposes miniaturizing antennas using a reflector-array surface with a fixed-polarization feed line. Additionally, (Al-Naiemy et al., 2018) introduces a frequency-reconfigurable MTS antenna operating at 5 GHz for long-range communication systems. This antenna, integrated with a frequency selective surface, is implemented with planar technology, enhancing simplicity and efficiency.

Numerous researchers have explored the integration of metasurface layers to improve antenna performance. For instance, (Alnaiemy et al., 2018) introduces an MTS-based design aimed at enhancing antenna gain. Similarly, (Elwi et al., 2011) proposes a high-gain antenna utilizing a three-layer configuration, achieving significant gain enhancements without resorting to smart applications. In (Kai et al., 2022), authors investigate the design of a high-gain wideband antenna incorporating a Gaussian lens. Furthermore, (Sravya & Kumari, 2018) explores the utilization of a Fabry-Perot cavity to enhance antenna gain, particularly for millimeter waves.

Distinctive modulation techniques are also under scrutiny. (Che et al., 2010) discusses near-field direct antenna modulation for designing time modulation communication links. Additionally, research efforts focus on tailoring antenna gain through MTS array dimension adjustments. (Pirhadi et al., 2012) presents a design for a high-gain antenna with variable gain achieved by altering MTS array dimensions, later elaborated upon in (Kodera, 2018).

Analytical approaches utilizing Fourier optics and ray tracing are detailed in (Hosseini et al., 2014; Liu et al., 2015), respectively, to examine MTS operation for gain enhancements. Recent advancements, documented in (Al-Dulaimi et al., 2020; Barnes & Greenebaum, 2007; CST Microwave Studio, 2018; Elachi & Van Zyl, 2006; Elwi, 2019; Elwi et al., 2020; Kizer, 2013; Yao et al., 2014), center around smart coded MTS layers acting as reflectors. Notable examples include (Kodera, 2018), which designs an MTS for an 8-phase shift keying wireless transmitter, and (Elwi et al., 2020), proposing amplitude-shift keying modulation through switchable MTS in THz applications.

Further innovations encompass phase shift keying via smart MTS with varactor diodes (Al-Dulaimi et al., 2020), reprogrammable holograms based on one-bit MTS for imaging applications (Kizer, 2013), and microwave imaging using 2-bit programmable MTS (Elachi & Van Zyl, 2006). Active MTS at THz frequencies is also explored to improve scattering diffusion (Barnes & Greenebaum, 2007; CST Microwave Studio, 2018; Elwi, 2019).

However, the applicability of these approaches is limited to specific antenna types, primarily reflector arrays. Consequently, their results may not directly apply to planar antennas, including microstrip structures. Subsequent research (Kizer, 2013) has addressed this limitation by employing MTS layers without restrictions on antenna type, unlocking several advantages. Programmable MTS structures offer exceptional capabilities in controlling antenna beamforming parameters such as amplitude, main lobe direction, and beam width (Elwi, 2019). It has been demonstrated that electromagnetic wave modulation can be achieved by electrically varying the distribution of coefficients (transmission or reflection) across the MTS (Elwi et al., 2019).

The study presented in this paper investigates the intricate relationship between metasurface (MTS) configurations and wireless channel performance. By analyzing bit-error-rate (BER) and channel capacity (CC), we aim to elucidate how variations in MTS unit-cell density affect these critical metrics.

The MTS layer used in the study comprises an array of identical unit-cells, which are implemented from overlaying circular, square, and Jerusalem cross microstrip-line elements. This novel MTS unit-cell layer is strategically positioned in front of an antenna design, resembling an H-shape checkerboard. The proposed MTS layer in this arrangement is shown to spatially focus the antenna's radiation and thereby enhance its gain performance. We rigorously assess the antenna's performance across a range of unit-cell densities.

SHABEEB KAMIL ET AL. 2 of 15



To validate our analytical findings, we conduct experimental tests, which yield results closely aligned with our predictions. This validation underscores the reliability and effectiveness of our proposed methodology.

2. Ray Tracing and Optical Concept Analysis

The proposed MTS layer design can be investigated using an analytical approach, as the behavior of an MTS layer is very similar to that of an optical lens, with a diffraction margin criterion that essentially defines the theoretical limits. The behavior of the MTS layer can be interpreted through the lens of optical theory, as it enables beam focusing and steering. This effect concentrates electromagnetic energy in a specific direction like how an optical lens focuses light, which enhances antenna gain and narrows the beamwidth (Battaglia et al., 2019, Battaglia, Morabito, Sorbello & Isernia, 2020, Battaglia, Morabito, Palmeri & Isernia, 2020). Therefore, it is useful to merge electromagnetic field theory and optical tracing theory into a hybrid computational algorithm (Battaglia, Morabito, Sorbello & Isernia, 2020, Battaglia, Morabito, Palmeri & Isernia, 2020; Battaglia et al., 2023; Bui et al., 2021). In this process, we focused the analysis on optical signal array processing (Balanis, 2016). Based on the array analysis of a homogeneous MTS array, the overall performance can be evaluated from the impulse response of the particle unit cell in convolution with the array function (Alnaiemy et al., 2018). In the case of periodical MTS arrays, an expression for the array function can be directly derived from the Fourier domain in 2D form (Balanis, 2016) and is given by:

$$F_{\rm SL}(v_x, v_y) = \left[\frac{\sin(\frac{\pi x X}{\lambda d}(N+1))}{\sin(\frac{\pi x X}{\lambda d})} \right]^2 \tag{1}$$

The variables in Equation 1 are defined in (Balanis, 2016). It is clear from this relationship the array function is affected by the separation between the unit-cells and the periodicity number. The unit-cell impulse response function can be determined by Equation 1, where the boundary condition is chosen in a way that zero diffraction occurs at the edges of MTS layers. The impulse response of an individual MTS unit cell is crucial in determining the overall behavior of the array, including its ability to concentrate beams emerging in a specific direction. This property is important for various applications in beamforming and signal processing, where precise control over the directionality of electromagnetic waves is required. The detailed analysis of the impulse response helps in designing MTS arrays that can efficiently focus or steer beams, enhancing their performance in communication systems and other technologies (Achouri et al., 2020).

The main lobe of the antenna system can be directed perpendicular to the proposed MTS surface, ensuring that the emerging electromagnetic waves are paraxial. Consequently, side lobes in the antenna pattern can be reduced by optimizing the design to minimize diffraction effects. The number of unit-cells, N can be calculated by Equation 2,

$$N = \frac{\lambda d}{2xX} - 1 \tag{2}$$

where *X* is the largest dimension of the unit-cell, *x* is the periodical repetition distance between unit-cell centers, λ is the operating wavelength and *d* is the largest dimension of the total array. It should be noted that we are not considering the effects of the unit-cell response in terms of scattering and electrical dimensions. As a result, the calculated number of unit cells may be a non-integer. In such cases, the nearest integer value is used. Based on ray tracing analysis inspired by optical theory (Elwi et al., 2011), the operational principles of MTS layers are explored for lenses mounted in front of the antenna. The synthesis of the proposed MTS design follows two considerations: First, the dimensions of the proposed MTS layer are equal to or smaller than those of the microstrip antenna ground plane, which helps to reduce side lobe levels. Second, the phase difference between two neighboring unit cells on the MTS layer diagonal is designed to be $\sqrt{2} \pi$ radian. The phase difference, ψ_p , shown in Figure 1 on the metasurface layer can be calculated by (Abdelrahman et al., 2017)

$$\psi_p = \psi_i - \psi_\circ = k[R_i - (\vec{r}_i \cdot \hat{r}_\circ)] \tag{3}$$

SHABEEB KAMIL ET AL. 3 of 15



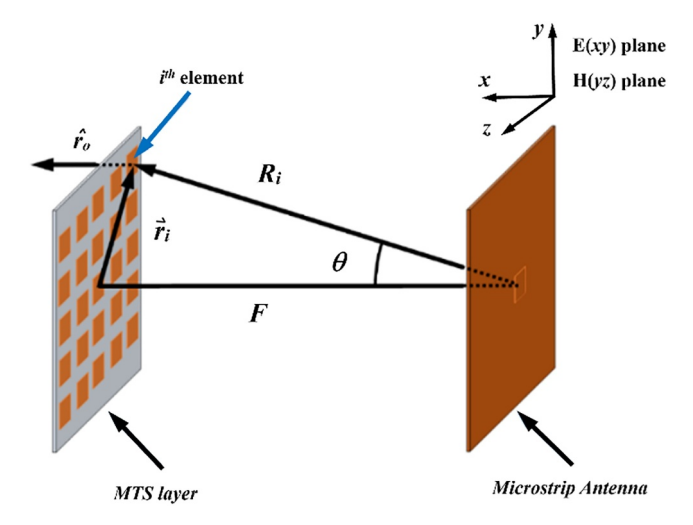


Figure 1. Ray tracing-based phase difference.

where k is the wavenumber in free space, R_i is the distance between the centers of the ith element and phase center, \vec{r}_i is the position vector of ith element and \hat{r}_o represents the direction vector of the main beam. The term ψ_p , which is equal to $\psi_i - \psi_o$, represents the phase difference between the normal incident ray and extreme emerging ray.

Since \vec{r}_i and \hat{r}_o are almost perpendicular at the broadside direction, θ becomes very small. Moreover, the antenna gain is inversely proportional to both θ and φ angles, which are the elevation angle at the E-plane, and φ is the azimuth angle at the H-plane (in degrees), respectively (Balanis, 2016).

$$G \propto \frac{1}{\theta \varphi}$$
 (4)

During the analysis, θ is assumed to be equal to φ to obtain symmetry in the radiation pattern. As anticipated, higher antenna gain is obtained with the smaller values of θ and φ . The focal length of the MTS layer, which can be calculated by using Equation 5, is also dependent on angle θ .

$$F = \frac{D/2}{\tan \theta} \tag{5}$$

Here, D is the diagonal distance of the MTS layer and it can be set to $\sqrt{2}$ W. θ is the incident wave angle on the MTS layer. The variation of the focal distance as the function of θ parameter is shown in Figure 2. It is observed that the larger the angle of incidence the lower the focal distance. For the proposed MTS layer, the focal distance is 60 mm.

Utilizing metasurface layers to enhance the gain of directive antennas is often challenging due to the complexity of converging electromagnetic beams over a narrow spatial range. However, for low-gain antennas, which are characterized by a wide beamwidth, employing MTS layers can be advantageous. This is because low-gain antennas require a shorter focal length to maximize antenna gain, making it easier to achieve the desired beam shaping and focusing with MTS layers. By optimizing the design and configuration of these metasurface layers, it is possible to effectively enhance the performance of low-gain antennas, improving their overall efficiency and functionality.

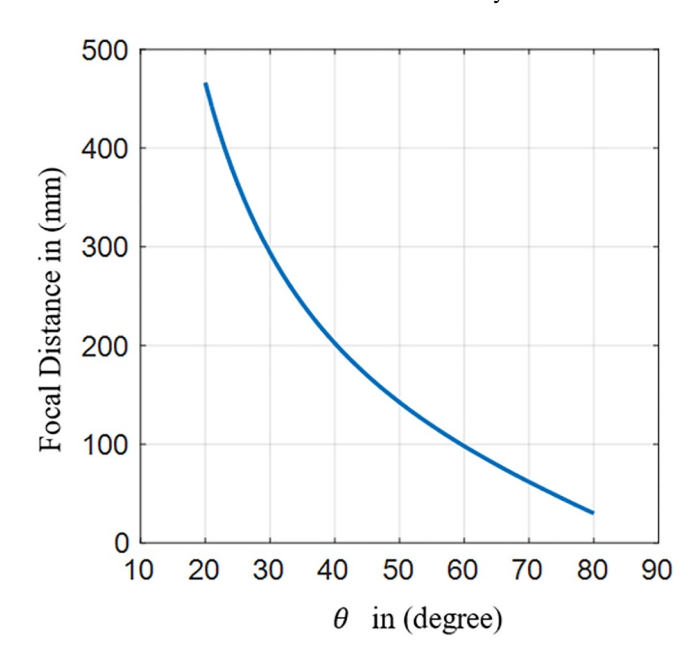


Figure 2. Focal distance variation as the function of θ .

The ray tracing procedure applied for the analysis of the microstrip antenna with the MTS surface is illustrated in Figure 3. The microstrip antenna, which serves as the feed antenna, is the source of electromagnetic waves. The rays diverging from the patch surface are shown by blue solid lines in Figure 3a. These rays, emerging from the microstrip antenna, impinge on the back side of the MTS layer. The width of the MTS layer captures the incident rays within the angle θ_1 , as shown in Figure 3b. The refracted wave from the MTS layer then propagates in free space at angle θ_2 .

By applying ray tracing on the extreme rays in Figure 3c the focal length can be significantly affected by incident angle θ_1 according to Snell's law. The angle θ_2 of the refracted signal is given by

$$\theta_2 = \sin^{-1} \left[\left(\frac{n_1}{n_2} \right) \sin \theta_1 \right] \tag{6}$$

where n_1 is the refractive index of free space ($n_1 = 1$) and n_2 is the refractive index of the MTS unit-cell. Although the refracted rays emanating from the MTS layer have better focusing capability compared to a single microstrip antenna, as shown in Figure 3d, some of the incident rays from the microstrip antenna are reflected from the bottom side of the MTS layer due to total internal reflection.

SHABEEB KAMIL ET AL. 4 of 15



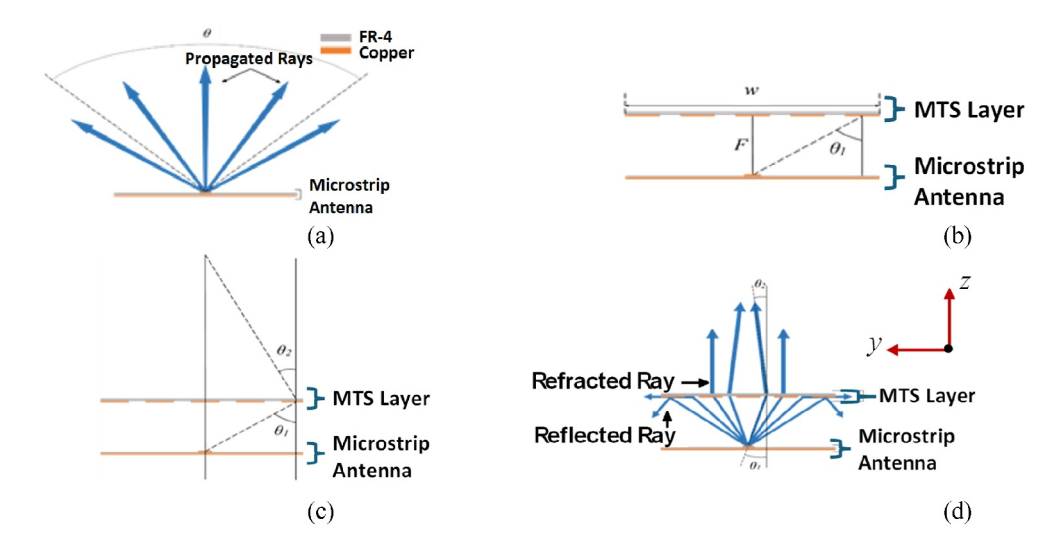


Figure 3. Ray tracing analysis: (a) the rays from the microstrip antenna, (b) rays at the MTS layer edges, (c) beam refraction at the MTS edges, and (d) refracted and reflected rays from the MTS layer.

The blue curve in Figure 4 is obtained using Equation 6. It shows the variation of refraction angle as the function of refraction index. Figure 4 shows that when n_2 approaches negative infinity, θ_2 approaches zero, resulting in a paraxial beam. Thus, the gain enhancement of the antenna consisting of the MTS layer is dependent on the value of n_2 . This characteristic of the n_2 parameter enables the design of antennas with enhanced gain.

MTS focal length and angle of incidence relation given in Equation 5 can be rewritten with respect to n_2 as follows:

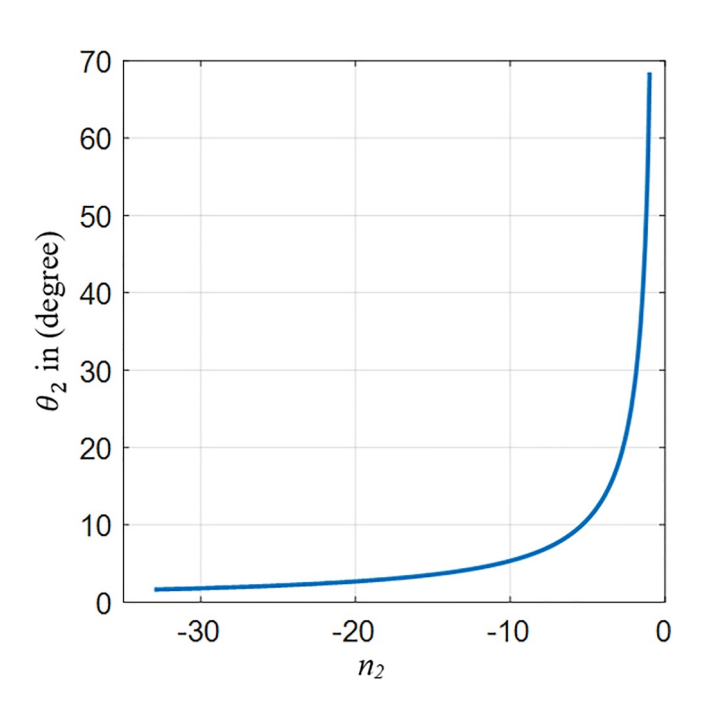


Figure 4. Variation of the transmission angle as the function of n_2 .

$$F = \frac{D/2}{\tan(\sin^{-1}[(n_2/n_1)\sin\theta_2])}$$
 (7)

If the θ_2 is chosen to be 2°, n_2 becomes less than -1. In Figure 5, focal distance variation is shown as the function of n_2 . Higher values of focal distance are observed for closer to zero values of n_2 .

The Fresnel reflection coefficient of the parallel and perpendicular polarized wave components of the MTS layer can be calculated by using Equations 8 and 9, respectively.

$$\Gamma_{/\!/} = \frac{n_1 \cos \theta_2 - n_2 \cos \theta_1}{n_1 \cos \theta_2 + n_2 \cos \theta_1} \tag{8}$$

$$\Gamma_{\perp} = \frac{n_1 \cos \theta_1 - n_2 \cos \theta_2}{n_1 \cos \theta_1 + n_2 \cos \theta_2} \tag{9}$$

The variation in the reflection coefficient at parallel and perpendicular polarizations are shown in Figures 6a and 6b, respectively, for $n_2 = -10$, -20 and -30. Total internal reflection is observed for incident rays propagating from rare medium to denser medium, irrespective of whether the polarization is perpendicular or parallel.

SHABEEB KAMIL ET AL. 5 of 15

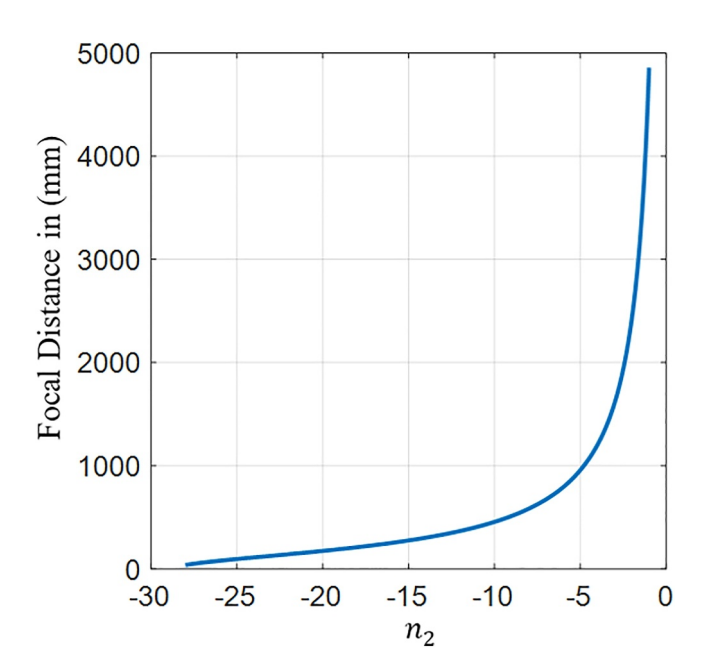


Figure 5. Variation of the focal distance as the function of n_2 .

3. Design of the Antenna With Enhanced Gain Characteristics

3.1. MTS Layer

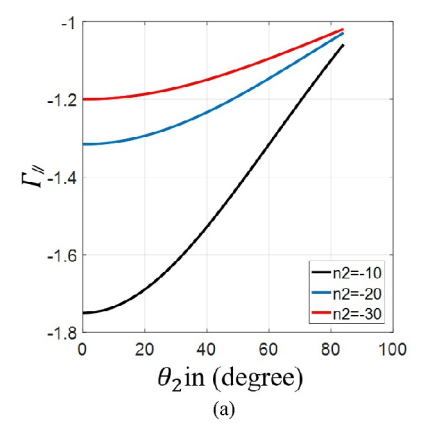
Three different geometries are used in the MTS layers, each based on an array of 5×5 unit-cells. The selection of circular, square, and Jerusalem cross unit-cell geometries was guided by their well-documented electromagnetic characteristics in terms of resonant behavior, transmission/reflection control, and beam shaping capability. Circular and square loops are known for their simple geometry and efficient surface current distribution, offering good impedance matching and broad resonance profiles (Manteghi, 2016; Park et al., 2016). The Jerusalem cross structure, on the other hand, provides a more complex current path, leading to sharper resonances and higher effective refractive index, making it ideal for beam focusing applications (Elwi et al., 2011, 2020). These designs were also chosen based on previous studies that demonstrated their ability to reduce back-radiation, minimize diffraction losses, and enhance antenna gain (Elwi, 2019). Including this combination allows us to explore and validate the performance enhancement in terms of BER and CC due to varying field manipulation capabilities of each geometry.

The layers are constructed from well-known designs reported in the literature. By using MTS layers with unit cells consisting of three different geometries, the aforementioned theory is validated, and an antenna with enhanced gain

characteristics is established. The upper layer is constructed from a Jerusalem Cross section, while the bottom layer is based on circular and square loops. These designs have been discussed in references (Manteghi, 2016; Park et al., 2016).

In this work, we introduce a novel analysis to examine the effects of different unit-cell designs on channel performance. Each structure within the unit-cell is parametrically studied to determine its effects on BER (Bit Error Rate) and CC (Channel Capacity) performance. Figure 7 shows the proposed MTS layers, with maximum unit-cell dimensions of 32 mm. The proposed MTS layer, constructed with an array of 5×5 unit-cells, reduces total internal reflection, which causes severe back radiation, and minimizes diffraction losses due to electromagnetic fringing from the layer edges, as discussed in reference (Elwi et al., 2011). These improvements positively affect BER and CC values. The proposed MTS layer occupies an area of approximately $160 \times 160 \text{ mm}^2$.

The proposed MTS layers are positioned at a distance D from the microstrip patch antenna, a placement crucial for determining antenna gain. This distance is chosen to match the focal length of the lens, typically around $\lambda/4$ at the resonant frequency. This choice mitigates total internal reflection when waves transition from a high-density,



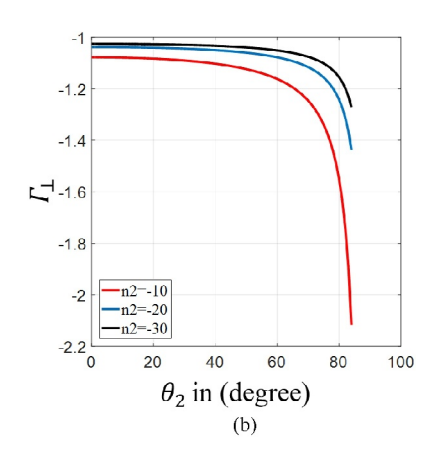


Figure 6. The reflection coefficient of the EM wave components of the MTS layer under the following polarization conditions: (a) parallel, and (b) perpendicular.

SHABEEB KAMIL ET AL. 6 of 15



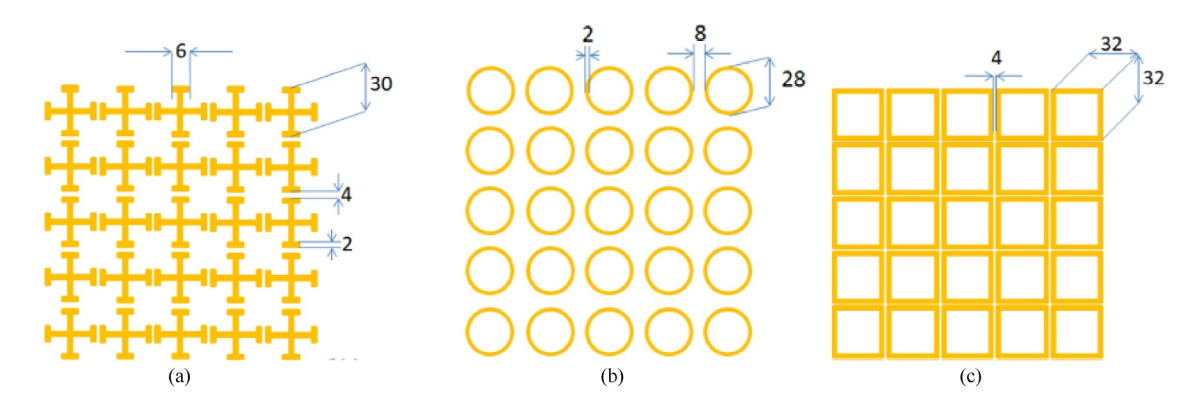


Figure 7. The proposed MTS layers: (a) Jerusalem cross, (b) Circular loop, (c) Square loop. All dimension units are in millimeters.

high-refractive-index medium to a lower-density, lower-refractive-index medium, a limitation noted in the numerical lens aperture (Che et al., 2010).

The MTS structure acts akin to a microwave lens, enhancing electric field intensity in specific directions to achieve a high numerical aperture (Manteghi, 2016). This is achieved by increasing the absolute refractive index value | n_{MTS} | of the proposed layers (Al-Dulaimi et al., 2020). The numerical aperture (NA) of wave propagating in free space toward the proposed MTS layer is given by

$$NA = \sqrt{n_{MTS}^2 - n_o^2} \tag{10}$$

The numerical aperture directly impacts antenna gain and affects the system's bit error rate (BER) and channel capacity (CC). The configuration of a 5×5 unit-cell array will illustrate these effects in the subsequent section.

Unit-cell density is a fundamental parameter in metasurface design as it determines the surface's ability to approximate a continuous phase profile. A higher density of unit-cells effectively reduces spatial quantization errors, thereby minimizing unwanted diffraction and scattering at the metasurface edges. This leads to smoother phase transitions and better beam shaping, which is especially crucial for maintaining narrow beamwidth and high gain. In our study, increasing the unit-cell density from 1×1 to 7×7 significantly reduced the total internal reflection and side-lobe levels, as observed in both simulation and measurement. These findings are consistent with prior work (Al-Naiemy et al., 2018; Henthorn et al., 2017a, 2017b), which showed that higher metasurface resolution leads to reduced edge diffraction and improved directional radiation. Additionally, a denser array reduces inter-cell spacing below the wavelength, which suppresses higher-order diffraction modes and enables more effective wavefront manipulation, resulting in improved BER and CC performance.

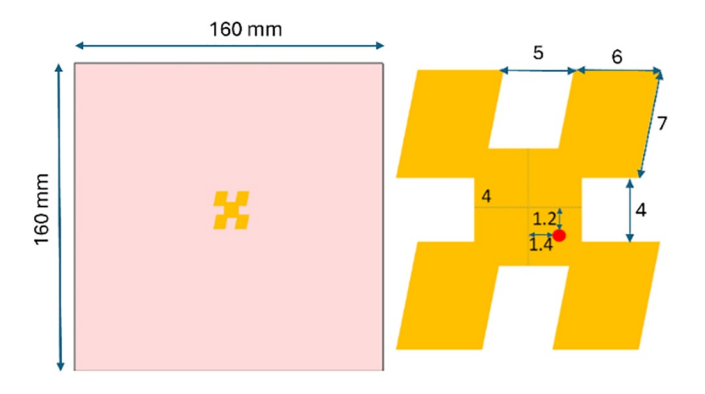


Figure 8. Proposed H-shaped checkerboard patch antenna. Dimensions annotated are in millimeters.

3.2. Antenna Design

In this section, we discuss the design of the proposed microstrip patch antenna, depicted in Figure 8. The patch has an H-shaped checkerboard arrangement, with surface currents generating circular polarization (Abdelrahman et al., 2017). The design of this patch structure is based on a traditional square patch with sections removed. The antenna was excited by a coaxial probe positioned at a 45° angle to the patch's symmetry axis. Placing the feed at 45° to the axis of symmetry allows the excitation of two orthogonal modes (TE modes) in the patch antenna, leading to circular polarization. Designed to operate at 5.5 GHz, this antenna serves as the feed for the MTS layer, which combines three array structures: Jerusalem cross, circular loop, and square loop. To minimize fringing effects from the substrate edges, the ground plane's physical size matches that of the MTS layer (Alnaiemy et al., 2018). The patch is printed on an FR4 substrate with a dielectric constant (ε_r) of 4.3 and a thickness of 1.6 mm. The size of the patch is $0.3\lambda_o \times 0.0.3\lambda_o$, where λ_o is free-space wavelength at 5.5 GHz.

SHABEEB KAMIL ET AL. 7 of 15



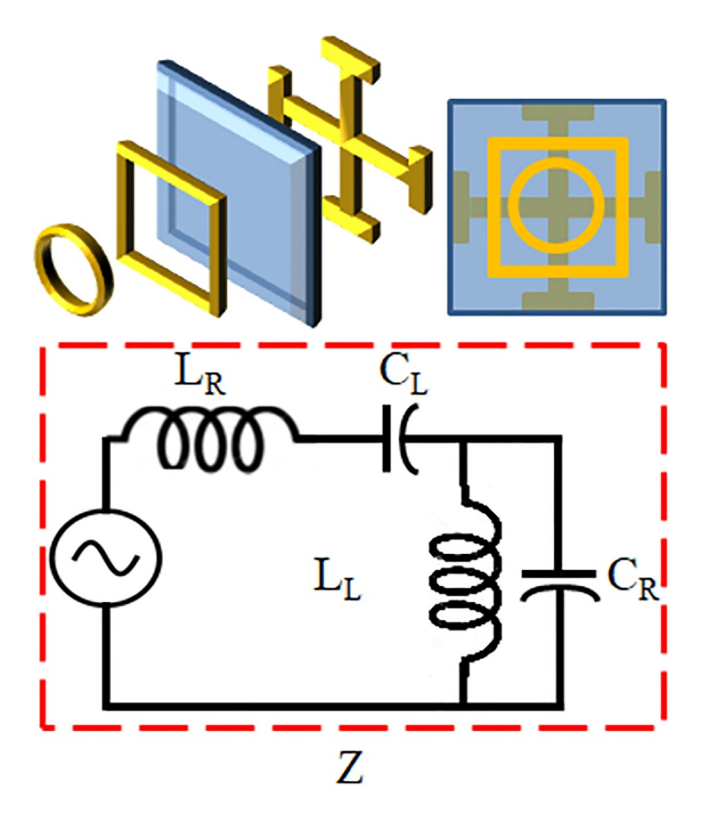


Figure 9. Simplified equivalent circuit of the MTS unit-cell.

4. MTS Unit Cell Operation

The electromagnetic properties of the proposed MTS layer are characterized analytically by using a transmission line model and numerically with full wave analysis tool (Alnaiemy et al., 2018). A single circuit model with different lumped element values is assumed. This assumption reduces the complexity of the analysis and represents a reasonable approximation, where the group velocity and phase change are asymptotically parallel with negligible intersection at infinity. Therefore, the effects of impinging fields can be neglected, and it is assumed that all the proposed unit-cells have the same circuit model. However, the values of the lumped element of each circuit model are different according to the slope variation of that asymptotic. The circuits are derived based on Left-Hand (LH) and Right-Hand (RH) branches. These branches are considered in the representation of the LH and RH properties.

The simplified circuit model of the proposed MTS unit-cell configuration is depicted in Figure 9. It is important to mention that the unit-cell is a combination of three different structures as illustrated in the figure. The effects of the LH branch are represented by the inductor (L_L) and capacitor (C_L) elements. On the other hand, the effects of RH branch are described by inductive (L_R) and capacitive (C_R) elements. Lumped element values of the equivalent circuit model of the MTS unit-cell are listed in Table 1.

Electromagnetic characterization of the proposed unit-cell was analyzed numerically using CST MWS (Kizer, 2013). During the simulations, the MTS unit-cell was positioned at the center of a virtual waveguide, as shown in Figure 10a. A perfect magnetic conductor boundary was chosen for the side walls of the box, while a perfect electric conductor boundary was assigned to

the top and bottom walls. The TEM-mode wave was excited by the two waveguide ports placed parallel to the top and bottom surfaces of the MTS layer.

The proposed unit-cell is constructed from a combination of Jerusalem cross, circular, and square loop configurations. Conductor traces with air gaps were added between the unit cells. The equivalent circuit model of this structure is shown in Figure 10b. Figure 10c shows the simulated reflection and transmission coefficients using ADS software. The dips in the S_{11} response correspond to the frequencies at which the metamaterial unit cell is well-matched to the incident wave, meaning that the reflection coefficient is low. The isolation (S_{12}) between the two ports at the resonant frequencies is better than -6 dB, which suggests relatively weak coupling. This reduced isolation is due to the absence of a ground plane, which would typically provide additional shielding and help to reduce coupling between ports. The values of the lumped circuit elements listed in Table 1 were calculated using Equations 11 and 12, which are based on the geometrical dimensions of the MTS unit-cell (Elwi et al., 2019).

$$C_R \approx \frac{0.264 \,\epsilon_r + 0.3755}{\ln(7.475 \,F/L)}$$
 (11)

$$L_R \approx \ln(7.475 \, F/L)^2 \tag{12}$$

 Table 1

 Lumped Elements of the Proposed MTS Unit-Cell

Symbol	Jerusalem cross	Circular	Square
C_R (pF)	0.08	0.1	1.06
L_R (nH)	11.3	10.1	13.05
C_L (pF)	0.09	0.05	1.03
L_L (nH)	2.13	1.24	2.55

 C_R is mostly due to the fringing capacitance that was calculated according to the methodology described in (Elwi et al., 2019). As inductance is related to the focal length, it is evident from Equations 11 and 12 that the focal length will be impacted by the magnitudes of C_R and L_R . L is the major dimension of the MTS unit-cell and the periodical gap, and in this case, it is 32 mm. From the equivalent circuit model, shown in Figure 10b, the resonant frequency of the unit-cell (f_r) can be calculated using Equation 13. The reflection and transmission coefficient of the MTS unit-cell using ADS and CST electromagnetic analytical tools is verified in Figure 10c.

SHABEEB KAMIL ET AL. 8 of 15



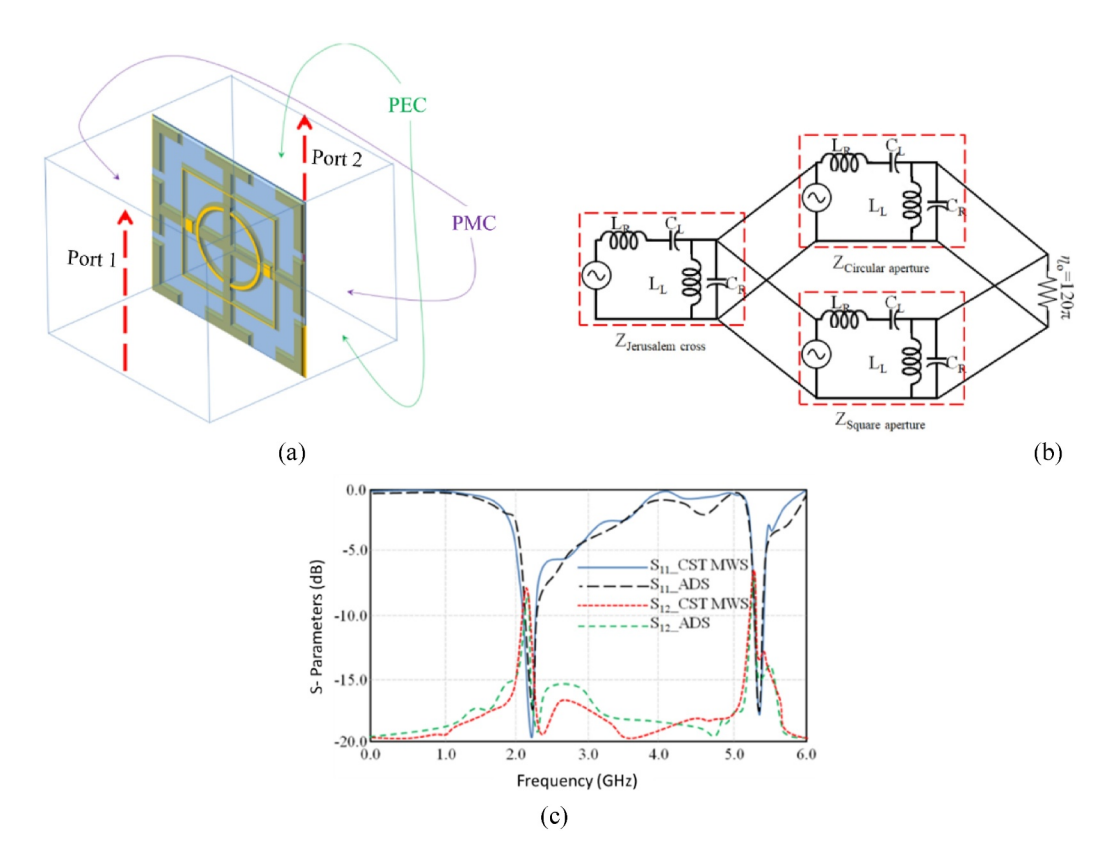


Figure 10. MTS unit-cell analysis: (a) Numerical setup, (b) Equivalent circuit model, and (c) S-parameters.

$$f_r = \frac{1}{2\pi} \sqrt{\frac{L_L + C_L}{L_L C_L (L_R + C_R)}}$$
 (13)

5. Performance Evaluation of the Antenna With MTS Layer

In this section, we verify the impact of including a metasurface (MTS) layer on the radiation performance of an antenna. The MTS layer here consisted of an array of unit-cells with three different structures, positioned above a microstrip antenna. The effect of varying the gap (F), defined in Figure 1, between the MTS layer and the antenna from 10 to 40 mm, in steps of 10 mm, was analyzed. The antenna's performance, measured in terms of reflection-

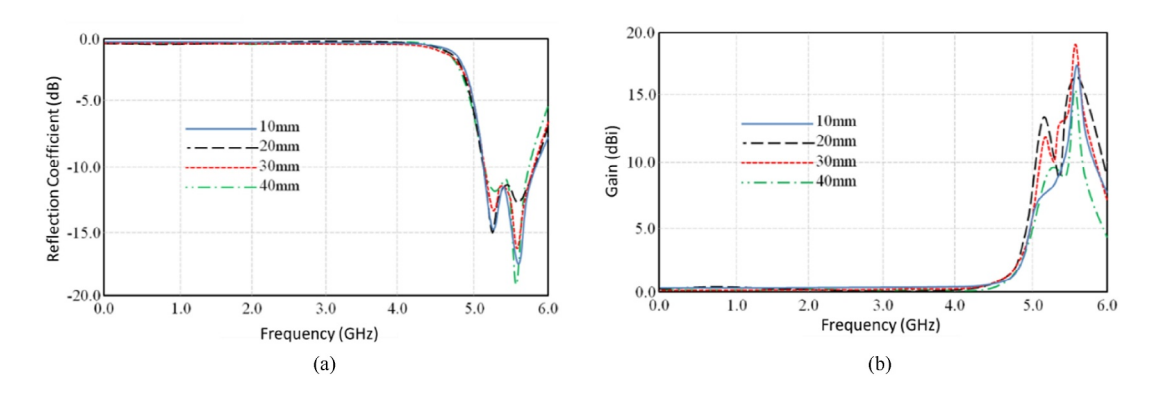


Figure 11. Performance of the antenna with MTS layer at various gap separation (F) between the antenna and MTS layer: (a) Reflection coefficient (S_{11}) , (b) Gain.

SHABEEB KAMIL ET AL. 9 of 15

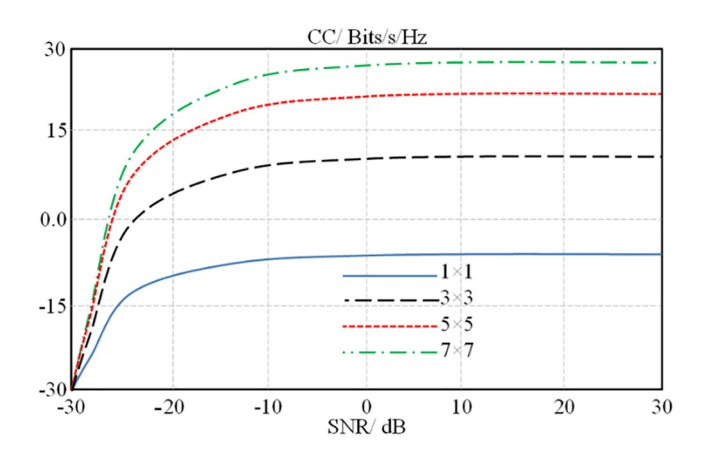


Figure 12. Channel capacity variation with respect to the proposed MTS layer configuration variation.

coefficient and antenna gain, is shown in Figure 11a. The proposed antenna exhibits a resonance response centered around 5.5 GHz, with the reflection-coefficient staying below -10 dB at the resonant frequency for all gap distances. Although significant variation in the reflection-coefficient (S_{11}) is not observed at 5.5 GHz, Figure 11b demonstrates that the antenna gain is affected by the gap distance. Specifically, the gain of the antenna increases to 18 dBi when the gap is 30 mm.

6. Channel Performance

6.1. Channel Capacity Variation

The channel performance of the MTS layer with $n \times n$ unit-cells was investigated. A numerical analysis was conducted to observe the effects of changing the number of unit-cells constituting the proposed MTS layer. MTS layers with n = 1, 3, 5, and 7 were considered. The results show that a narrower beamwidth is obtained with an increased number of unit-cells.

These improvements are attributed to the significant reduction in total internal reflection of the incident rays as the array size increases, as described in (Al-Naiemy et al., 2018). In smaller arrays, incident rays are more likely to undergo internal reflection, which can cause undesired scattering and broaden the beamwidth. By increasing the number of unit-cells, the structure becomes more capable of directing the rays efficiently, thus narrowing the beamwidth.

Additionally, the refracted rays undergoing diffraction from the array edges are significantly reduced with a larger array size, as noted in (Yang et al., 2020). Diffraction from the edges of smaller arrays can lead to energy dispersion and reduced performance. Larger arrays mitigate this effect by offering a more continuous surface for wave propagation, enhancing overall directivity.

Furthermore, the gain is significantly affected by the location of the antenna relative to the top of the MTS layer. As the distance between the antenna and the MTS layer changes, it influences how effectively the MTS can enhance the antenna's radiation pattern.

The channel capacity of the proposed MTS layer-based antenna is shown in Figure 12 for array sizes of 1, 3, 5, and 7. It is observed that the channel capacity increases rapidly with increasing array size up to a signal-to-noise ratio (S/N) of -15 dB before stabilizing. The 7×7 array provides the best channel capacity as a function of S/N. This suggests that a larger array size not only improves the radiation characteristics but also enhances the antenna's ability to handle higher data rates, making it more efficient in communication applications.

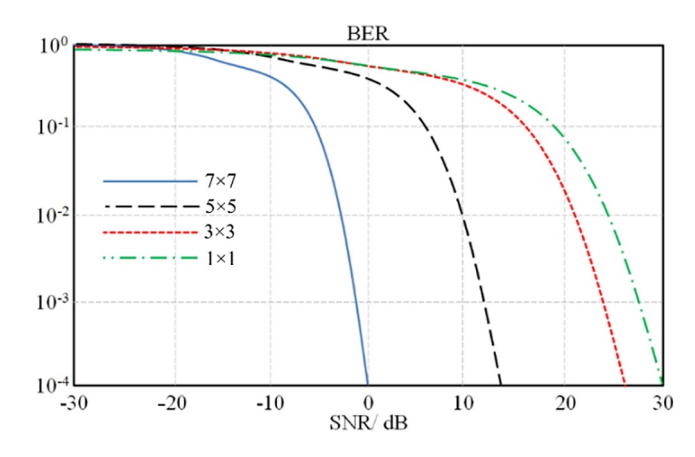


Figure 13. The calculated BER of different MTS layer configurations.

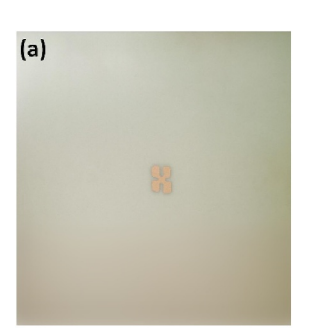
6.2. BER Variation

The Bit Error Rate (BER) of the MTS layer-based antenna was calculated by varying the signal-to-noise Ratio (SNR) from -30 to 30 dB. This analysis utilized white noise along with a random input binary stream, employing the Phase Shift Keying (PSK) modulation scheme. The evaluated BER for different array sizes is shown on Figure 13.

The results indicate that the proposed antenna with MTS layer having an array size 1×1 to 7×7 provide identical BER up to an SNR of -20 dB. However, for SNR greater than -20 dB the larger array size exhibits superior performance in terms of error rate, ensuring more reliable data transmission.

A lower BER signifies fewer errors in the received data, which is crucial for maintaining integrity and quality of communication. The 7×7 array size is particularly effective because they enhance the antenna's ability to mitigate the effects of noise and interference. This is achieved through the more extensive surface area of the larger array, which allows for better handling and focusing of the electromagnetic waves, thereby reducing the probability of errors.

SHABEEB KAMIL ET AL. 10 of 15



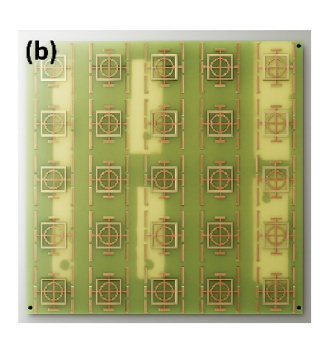


Figure 14. The fabricated antenna-based MTS layer prototype: (a) Antenna structure, and (b) MTS layer.

The enhanced BER performance can be attributed to several factors. Larger arrays help in shaping the radiation pattern more effectively, reducing side lobes and focusing the energy on the desired direction. This results in a stronger and clearer signal reception, which directly contributes to a lower BER. As discussed earlier, increasing the array size reduces internal reflections and edge diffractions. This reduction minimizes the scattering and dispersion of the signal, thereby enhancing the clarity and accuracy of the received data. The larger arrays are more capable of handling higher SNRs effectively. This capability ensures that the signal remains strong relative to the noise, leading to fewer errors in data interpretation.

7. Experimental Validation

The fabricated prototype of the proposed antenna system is presented in Figure 14, where part (a) shows the antenna structure and part (b) depicts the

corresponding metasurface (MTS) layer. Both components were fabricated on FR-4 substrates, a widely used material in PCB manufacturing due to its durability and favorable electrical properties. The fabrication process employed standard PCB chemical etching techniques, which involve selectively removing copper to form the required circuit patterns.

The MTS layer, shown in Figure 15, essential for manipulating electromagnetic waves and enhancing antenna performance, was fabricated using the same procedures to ensure precision and consistency with the antenna design.

To evaluate the performance of the fabricated system, key parameters were measured, including the S_{11} spectra, gain, and radiation patterns. The S_{11} parameter, which quantifies the reflected power from the antenna, is a critical indicator of impedance matching and overall efficiency. Measurements were carried out using a Vector Network Analyzer (Agilent PNA 8720 series).

Antenna gain, representing the effectiveness of converting input power into radiated energy in a specific direction, was also assessed. Higher gain values correspond to improved signal strength and communication range. In addition, radiation patterns were measured to analyze the directional distribution of the radiated power. All measurements were performed with the antenna mounted on a rotational holder inside an RF anechoic chamber, ensuring accurate characterization under minimal reflection and interference conditions.

The antenna's radiation performance was measured both without and with the MTS layer. To ensure minimal reflections and interference, the antenna was mounted on a rotational table within an anechoic chamber. The measurement system was calibrated using a reference antenna to ensure accuracy. A Vector Network Analyzer (VNA) was employed to measure the radiation and gain at various azimuthal and elevation angles. The radiation pattern was assessed by rotating the antenna and recording the radiated power at different angles in both the azimuth and elevation planes.

The simulated and measured S_{11} spectra, as well as the obtained gain performance over the 4–6 GHz range, are shown in Figure 15. This figure presents the S_{11} spectra of the antenna both with and without the proposed MTS layer. The proposed antenna resonates at around 5.5 GHz. With the inclusion of the MTS layer, the reflection coefficient is observed to broaden.

The measured radiation pattern without the MTS layer at 5.5 GHz is shown in Figure 15b. The E(xy) and H(yz) planes are defined in Figure 1. The radiation pattern with the MTS layer at 5.5 GHz is shown in Figure 15c. It is evident that with the MTS layer, the 3-dB beamwidth is significantly reduced. However, the antenna gain is notably increased by 18 dBi from 1 dBi to 19 dBi at 5.5 GHz in both azimuthal and elevation planes after applying the proposed MTS layer.

Experimental validation confirmed the key theoretical predictions regarding the resonant frequency and directional behavior of the antenna. The measured S_{11} spectra showed excellent agreement with simulations, exhibiting resonance at approximately 5.5 GHz and improved impedance matching. Furthermore, the radiation pattern measurements aligned with the predicted focusing effect of the metasurface, with observed narrowing of the main

SHABEEB KAMIL ET AL. 11 of 15



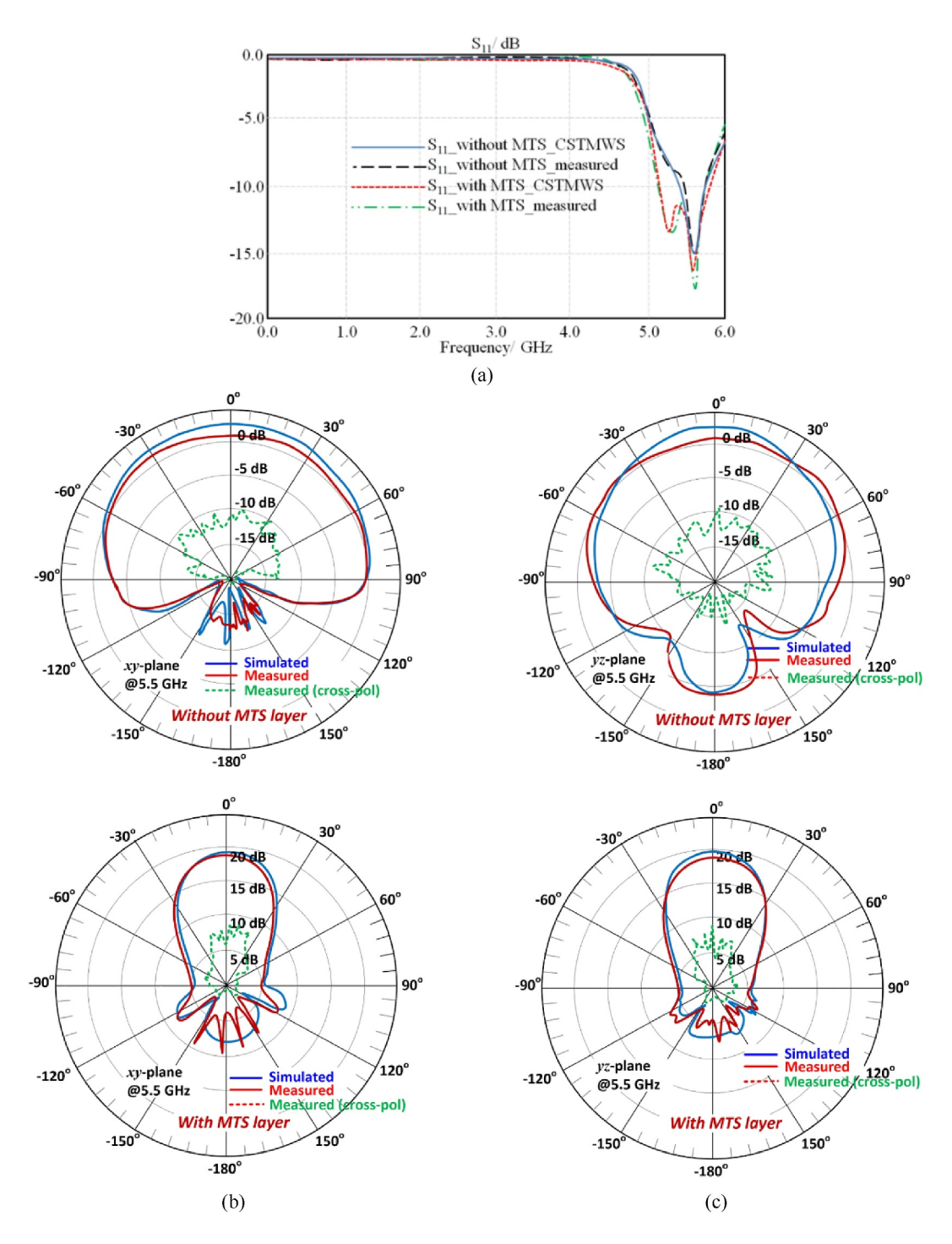


Figure 15. Measured performance of the proposed antenna system without and with the MTS layer: (a) S_{11} spectra, (b) Measured and simulated radiation patterns in the E(xy) plane without and with the MTS layer, and (c) Measured and simulated radiation patterns in the H(yz) plane without and with the MTS layer.

lobe and increased directivity. These results support the effectiveness of the proposed MTS design in practical implementation. A comparison summary is provided in Table 2.

Finally, the performance of the proposed antenna is comprehensively compared with several state-of-the-art designs reported in recent literature, as summarized in Table 3. This comparison includes key parameters such as operating frequency, substrate type, physical dimensions, normalized size in terms of the free-space

SHABEEB KAMIL ET AL. 12 of 15



 Table 2

 Summary of Theoretical and Experimental Antenna Performance

Parameter	Theoretical prediction	Experimental result	Agreement	Remarks
Resonant Frequency (GHz)	5.5 GHz	5.48–5.52 GHz	Yes	Minor shift likely due to fabrication tolerances
Reflection Coefficient (S_{11})	≤−10 dB at resonance	<-15 dB at 5.5 GHz	Yes	Indicates effective impedance matching
Antenna Gain Pattern	Directional with narrower beamwidth using MTS	Narrower beamwidth and higher directivity observed	Yes	Measured patterns validate theoretical focusing behavior
Channel Capacity	Predicted improvement with higher MTS density	Not experimentally measured	N/A	Remains part of theoretical analysis
Bit Error Rate (BER)	Lower BER with larger array size	Not experimentally measured	N/A	Simulation-based evaluation only

wavelength (λ_0) and realized gain. The proposed antenna operates at 5.5 GHz, is fabricated on a standard FR4 substrate, and occupies a compact area of $160 \times 160 \text{ mm}^2$, corresponding to $2.93\lambda_0 \times 2.93\lambda_0$.

In terms of gain performance, the proposed antenna achieves a substantial gain of 18 dBi, which is among the highest values reported in the compared studies. Most of the existing designs with comparable or lower gain values either utilize larger physical structures (Elwi et al., 2011; Kai et al., 2022) or more complex substrate materials such as Taconic or RO3003 (Elwi et al., 2011; Pirhadi et al., 2012), which may increase fabrication cost and complexity. While the design in (Babakhani et al., 2008) achieves a slightly higher gain, it requires significantly more physical space, making it less suitable for compact system integration.

Notably, several other antennas listed in the table, including (Christydass et al., 2023; Ghosh et al., 2023; Mellita et al., 2017; Sravya & Kumari, 2018), offer compact sizes but suffer from considerably lower gain (ranging from 0.5 dBi to 4.54 dBi), indicating a trade-off between size and radiation performance. The proposed design addresses this trade-off effectively by combining a reasonably compact size with high gain, achieved through the strategic use of a hybrid metasurface layer and optimized unit-cell configuration.

This balance between size and performance is particularly advantageous for practical wireless systems where form factor constraints are critical such as in IoT devices, vehicular radar, or portable communication equipment. Therefore, the proposed antenna not only advances performance metrics but also demonstrates meaningful design utility in real-world applications.

Table 3 *Comparison of the Proposed Work With the Other Published Results*

Ref.	f_r (GHz)	Dielectric substrate	Physical size (mm ²)	Size $(\lambda_0)^2$	Gain (dBi)
Alnaiemy et al. (2018)	2.45	FR4	240×240	1.96 × 1.96	5.1
Elwi et al. (2011)	2.65	Taconic	360×360	3.18×3.18	17.8
Kai et al. (2022)	5.8	$\varepsilon_r = 2.2$	77.6×77.6	1.5×1.5	11.5
Sravya and Kumari (2018)	5.8	FR4	50×50	0.97×0.97	1.2
Che et al. (2010)	11.38	Polymer	50×50	1.89×1.89	7.88
Pirhadi et al. (2012)	9.6	RO3003	63×63	2.02×2.02	6
Mellita et al. (2017)	5.2	FR4	50×50	0.87×0.87	4.54
Ghosh et al. (2023)	5.2	FR4	26×20	0.21×0.16	3
Christydass et al. (2023)	5.88	FR4	16×15	0.31×0.29	0.5
Abdelkarim et al. (2024)	5.8	FR4	131×34	0.39×0.11	7
Dhabal et al. (2025)	9.8	FR4	81×81	1.35×1.35	8.25
Present work	5.5	FR4	160×160	2.93×2.93	18

SHABEEB KAMIL ET AL. 13 of 15



8. Conclusion

This study demonstrates the effectiveness of integrating the proposed metasurface (MTS) configuration layer to enhance antenna performance. By incorporating this MTS layer, we achieved a significant increase in antenna gain, reaching 18 dBi at a center frequency of 5.5 GHz. This improvement was validated through optical ray tracing analysis and the development of an equivalent circuit model.

The optical ray tracing analysis provided critical insights into how the MTS layer influences the antenna's radiation characteristics. It was observed that the focused antenna beam and its beamwidth at the resonant frequency are significantly affected by the refractive index of the MTS layer. The refractive index, which determines the metasurface's ability to bend and manipulate electromagnetic waves, is closely related to the effective capacitance of the MTS layer. This relationship is essential as it dictates how effectively the MTS layer can concentrate and direct the antenna beam.

The introduction of the MTS layer resulted in a more highly directional beamwidth, enhancing the antenna's performance by making its beam more focused. This increased directionality directly impacts the antenna gain, as a more concentrated beam translates to higher signal strength in the desired direction. Consequently, the MTS layer's improved focusing capability leads to a notable increase in gain.

Furthermore, our findings reveal that expanding the array size of the MTS layer enhances performance in terms of channel capacity and error rate. Specifically, a larger array size improves data transmission reliability. This enhancement is due to the reduction in total internal reflection of the incident rays, which becomes more effective as the array size increases. By managing the incident waves more efficiently, the metasurface reduces signal loss and improves overall system performance.

Conflict of Interest

09205071 2019 1683472

The authors declare no conflicts of interest relevant to this study.

Data Availability Statement

No data were used or generated in the course of this study.

Acknowledgments References

Co-funded by the European Union. Views and opinions expressed are however those of the author(s) only and do not necessarily reflect those of the European Union or the European Research Executive Agency. Neither the European Union nor the granting authority can be held responsible for them. Besides that, this publication has emanated from research jointly funded by Taighde Éireann—Research Ireland under Grant 13/RC/2094_2, the European Union's Marie Sklodowska-Curie Actions under Grant 101126578 and was supported in part by University of Galway.

Abdelkarim, M., Gharsallah, A., & Faouel, R. (2024). Analysis and design of a high gain multiband antenna based on metamaterials for RFID applications. *International Journal of RF and Microwave Computer-Aided Engineering*, 2024(1), 1–20. https://doi.org/10.1155/2024/8948916

Abdelrahman, A. H., Yang, F., Elsherbeni, A. Z., & Nayeri, P. (2017). In *Space-fed array design method*, "analysis and design of transmitarray antennas (1st ed., pp. 7–8). San Rafael, California, USA: Morgan & Claypool.

Achouri, K., Salem, M. A., Badi, M. A., & Caloz, C. (2020). Metasurface-based beamforming and signal processing for communication systems. Journal of Electromagnetic Waves and Applications, 34(4), 123–135.

Al-Dulaimi, Z., Elwi, T. A., & Atilla, D. C. (2020). Design of a meander line monopole antenna array based hilbert-shaped reject band structure for MIMO applications. *IETE Journal of Research*, 66(1), 1–10. https://doi.org/10.1080/03772063.2020.1743207

Alibakhshikenari, M., Virdee, B. S., Azpilicueta, L., Naser-Moghadasi, M., Akinsolu, M. O., See, C. H., et al., (2020). A comprehensive survey of "Metamaterial Transmission-Line Based Antennas: Design, Challenges, and Applications", In *IEEE Access* (Vol. 8, pp. 144778–144808). https://doi.org/10.1109/access.2020.3013698

Alibakhshikenari, M., Ali, E. M., Soruri, M., Dalarsson, M., Naser-Moghadasi, M., Virdee, B. S., et al. (2022). A comprehensive survey on antennas on-chip based on metamaterial, metasurface, and substrate integrated waveguide principles for millimeter-waves and terahertz integrated circuits and systems, In *IEEE Access* (Vol. 10, pp. 3668–3692). https://doi.org/10.1109/access.2021.3140156

Alibakhshikenari, M., Babaeian, F., Virdee, B. S., Aissa, S., Azpilicueta, L., See, C. H., et al. (2020). A comprehensive survey on "Various decoupling mechanisms with focus on metamaterial and metasurface principles applicable to SAR and MIMO antenna systems", In *IEEE Access* (Vol. 8, pp. 192965–193004). https://doi.org/10.1109/access.2020.3032826

Al-Naiemy, Y., Elwi, T. A., & Lajos, N. (2018). Enhancing the microstrip antenna gain using a novel MTS lens based on a single layer. In *Proceedings of the 3rd colloquium on microwave communication*.

Alnaiemy, Y., Elwi, T. A., Lajos, N., & Zwick, T. (2018). A systematic analysis and design of a high gain microstrip antenna based on a single MTS layer. *Infocommunications Journal*, 10, 1–9.

Babakhani, A., Rutledge, D. B., & Hajimiri, A. (2008). Transmitter architectures based on near-field direct antenna modulation. *IEEE Journal of Solid-State Circuits*, 43(12), 2674–2692. https://doi.org/10.1109/jssc.2008.2004864

Solid-State Circuits, 43(12), 26/4–2692. https://doi.org/10.1109/jssc.2008.2004864

Balanis, C. A. (2016). Fundamental parameters and figures-of-merit of antennas," antenna theory analysis and design (4th ed., pp. 63–64). Wiley

& Sons. Hoboken, New Jersey, USA.
Barnes, F. S., & Greenebaum, B. (2007). Bioengineering and biophysical aspects of electromagnetic fields (3rd ed.). Taylor & Francis Group.

Boca Raton.

Battaglia, G. M., Bellizzi, G. G., Morabito, A. F., Sorbello, G., & Isemia, T. (2019). A general effective approach to the synthesis of shaped beams for arbitrary fixed-geometry arrays. *Journal of Electromagnetic Waves and Applications*, 33(18), 2404–2422. https://doi.org/10.1080/

SHABEEB KAMIL ET AL. 14 of 15



- Battaglia, G. M., Isernia, T., Palmeri, R., & Morabito, A. F. (2023). Four-beams-reconfigurable circular-ring array antennas for monopulse radar applications. *Radio Science*, 58(9), e2023RS007776. https://doi.org/10.1029/2023rs007776
- Battaglia, G. M., Morabito, A. F., Palmeri, R., & Isernia, T. (2020). Constrained focusing of vector fields intensity in near zone and/or complex scenarios as a low-dimensional global optimization. *Journal of Electromagnetic Waves and Applications*, 34(15), 1977–1989. https://doi.org/10.1080/09205071.2020.1801521
- Battaglia, G. M., Morabito, A. F., Sorbello, G., & Isernia, T. (2020). Mask-constrained power synthesis of large and arbitrary arrays as a few-samples global optimization. *Progress in Electromagnetics Research C*, 98, 69–81. https://doi.org/10.2528/pierc19082904
- Bui, L. T., Anselmi, N., Battaglia, G. M., Isernia, T., Rocca, P., & Morabito, A. F. (2021). Synthesis of wideband reconfigurable array antennas for monopulse radar applications. *Progress in Electromagnetics Research M*, 106, 179–189. https://doi.org/10.2528/pierm21090905
- Che, Y., Hou, X., & Zhang, P. (2010). Design of multiple FSS screens with dissimilar periodicities for directivity enhancement of a dual-band patch antenna. In *Proceedings of the 9th international symposium on antennas, propagation and EM theory*.
- Chen, X., Zhang, L., & Zhang, Q. (2021). Metasurface antennas: A review of fundamentals and applications to satellite communications. *IEEE Access*, 9, 96018–96033.
- CST Microwave Studio. (2018). [online]. Retrieved from https://www.cst.com
- Dhabal, B., Kumar, A., Nandi, A., & Basu, B. (2025). Metamaterial-based AMC antenna with reduced RCS and increased bandwidth for wireless X-Band applications. *International Journal of Communication Systems*, 38(5), 1–11. https://doi.org/10.1002/dac.70019
- Elachi, C., & Van Zyl, J. J. (2006). Introduction to the physics and techniques of remote sensing. Wiley. New York, NY, USA.
- Elsharief, M., Emran, A. A., Hassan, H., Sabuj, S. R., & Jo, H.-S. (2022). SLES: Scheduling-based low energy synchronization for industrial internet of things. *IEEE Sensors Journal*, 22(16), 16652–16661. https://doi.org/10.1109/jsen.2022.3188758
- Elwi, T. A. (2019). Printed microwave metamaterial-antenna circuitries on nickel oxide polymerized palm fiber substrates. *Nature Scientific Reports*, 9(2174), 1–14. https://doi.org/10.1038/s41598-019-39736-8
- Elwi, T. A., AL-Hussain, Z. A., & Tawfeeq, O. (2019). Hilbert metamaterial printed antenna based on organic substrates for energy harvesting. *IET Microwaves, Antennas & Propagation*, 12(4), 1–8.
- Elwi, T. A., Al-Rizzo, H. M., Bouaynaya, N., Hammood, M. M., & Al-Naiemy, Y. (2011). Theory of gain enhancement of UC-PBG antenna structures without invoking Maxwell's equations: An array signal processing approach. *Progress in Electromagnetics Research B*, 34, 15–30. https://doi.org/10.2528/pierb11062709
- Elwi, T. A., Jassim, D. A., & Mohammed, H. H. (2020). Novel miniaturized folded UWB microstrip antenna-based metamaterial for RF energy harvesting. *International Journal of Communication Systems*, 1(2)
- Etman, A. M., Abdalzaher, M. S., Emran, A. A., Yahya, A., & Shaaban, M. (2025). A survey on machine learning techniques in smart grids based on wireless sensor networks. *IEEE Access*, 13, 2604–2627. https://doi.org/10.1109/access.2024.3524097
- Ghosh, K., Chandra, A., Kumar, R., Shah, A., & Chakraborty, U. (2023). CRLH-TL-loaded metamaterial antenna with frequency band and polarization reconfigurability. *International Journal of Communication Systems*, 37(3), 1–10. https://doi.org/10.1002/dac.5665
- Glover, I., & Grant, P. (2010). Bandpass modulation of a carrier signal," digital communications (3rd ed., pp. 390-449). Prentice Hall.
- Henthorn, S., Ford, K., & O'Farrell, T. (2017a). Frequency selective surface loaded antenna for direct antenna modulation. *Proc. on Antennas and Propagation (EUCAP)* (pp. 731–734). https://doi.org/10.23919/eucap.2017.7928325
- Henthorn, S., Ford, K. L., & O'Farrell, T. (2017b). Bit-error-rate performance of quadrature modulation transmission using reconfigurable frequency selective surfaces. *IEEE Antennas and Wireless Propagation Letters*, 16, 2038–2041. https://doi.org/10.1109/lawp.2017.2695008
- Hosseini, P., Wright, C. D., & Bhaskaran, H. (2014). An optoelectronic framework enabled by low-dimensional phase-change films. *Nature*, 511(7508), 206–211. https://doi.org/10.1038/nature13487
- Iskandarani, M. Z. (2024). Investigation of energy consumption in WSNs within enclosed spaces using beamforming and LMS (BF-LMS). *IEEE Access*, 12, 63932–63941. https://doi.org/10.1109/access.2024.3395932
- Kai, Shao, W., Ding, X., Wang, B. Z., & Jiang, B. (2022). Design of high-gain metasurface antenna based on characteristic mode analysis. IEEE Antennas and Wireless Propagation Letters, 21(4), 661–665, https://doi.org/10.1109/lawp.2022.3140326
- Kiani, A., Rajabzadeh, N., & Komjani, N. (2022). Compact and reconfigurable metasurface antenna for IoT applications. IEEE Internet of Things Journal, 9(15), 13220–13227.
- Kizer, G. (2013). Digital microwave communication engineering point-to-point microwave systems. John Wiley & Sons. New Jersey.
- Kodera (2018). Smart MTS with non-reciprocity for fog layer in IoT environment. In *IEEE international symposium on electromagnetic compatibility and 2018 IEEE Asia-Pacific symposium on electromagnetic compatibility (EMC/APEMC)* (pp. 912–914). Singapore.
- Liu, L., Kang, L., Mayer, T. S., & Werner, D. H. (2015). Hybrid metamaterials for electrically triggered multifunctional control. Nature Communications, 7(1), 13236. https://doi.org/10.1038/ncomms13236
- Manteghi, M. (2016). A wideband electrically small transient-state antenna. *IEEE Transactions on Antennas and Propagation*, 64(4), 1201–1208. https://doi.org/10.1109/tap.2016.2525828
- Mellita, A., Chandu, D. S., & Karthikeyan, S. S. (2017). Gain enhancement of a microstrip patch antenna using a novel frequency selective surface. In 2017 twenty-third national conference on communications (NCC). Chennai.
- Park, D., Kim, M., & Cho, D. (2016). Novel Single-RF MIMO system based on repetitive pulse width modulation. *IEEE Communications Letters*, 20(1), 165–168. https://doi.org/10.1109/lcomm.2015.2496171
- Pirhadi, A., Bahrami, H., & Nasri, J. (2012). Wideband high directive aperture coupled microstrip antenna design by using a FSS superstrate layer. IEEE Transactions on Antennas and Propagation, 60(4), 2101–2106. https://doi.org/10.1109/tap.2012.2186230
- Prasad Jones Christydass, S., Suresh Kumar, S., Nishok, V. S., Saravanakumar, R., Devakirubakaran, S., Deepa, J., & Sangeetha, K. (2023).
 Design of metamaterial antenna based on the mathematical formulation of patch antenna for wireless application. *International Journal of Antennas and Propagation*, 2023(1), 1–12. https://doi.org/10.1155/2023/2543923
- Qasem, N. (2024). Measurement and simulation for improving indoor wireless communication system performance at 2.4 GHz by modifying the environment. IEEE Access, 12, 96660–96671. https://doi.org/10.1109/access.2024.3426490
- Sravya, R. V., & Kumari, R. (2018). Gain enhancement of patch antenna using L-Slotted mushroom MTS. In 2018 conference on signal processing and communication engineering systems (SPACES), Vijayawada.
- Tantawy, Z. H., El, M., Mohamed, B., Emran, A. A., & Semeia, A. I. M. (2024). On the performance of FSO communication system with WDM and MIMO structure under different turbulent atmospheric conditions. *Journal of Optical Communications*, 45(1), s2133–s2149.
- Yang, Y., Chen, X., & Cui, T. (2020). Active metasurface-based wearable antenna for biomedical applications. *IEEE Transactions on Biomedical Circuits and Systems*, 14(2), 232–240.
- Yao, Y., Shankar, R., Kats, M. A., Song, Y., Kong, J., Loncar, M., & Capasso, F. (2014). Electrically tunable MTS perfect absorbers for ultrathin mid-infrared optical modulators. *Nano Letters*, 14(11), 6526–6532. https://doi.org/10.1021/nl503104n

SHABEEB KAMIL ET AL. 15 of 15